Intraband polarization and terahertz emission in biased semiconductor superlattices with full excitonic basis

Lijun Yang,[1] Ben Rosam,[2] Jean-Marc Lachaine,[3] Karl Leo,[2] and M. M. Dignam[1]
[1]*Department of Physics, Queen's University, Kingston, Ontario, Canada K7L 3N6*
[2]*Institut für Angewandte Photophysik, Technische Universität Dresden, 01062 Dresden, Germany*
[3]*Department of Physics, Lakehead University, Thunder Bay, Ontario, Canada P7B 5E1*
(Received 20 October 2003; published 15 April 2004)

We report theoretical and experimental results for the intraband dynamics of biased semiconductor superlattices excited by ultrashort optical pulses. The theoretical model used employs an excitonic basis that includes $1s$ and all higher-energy in-plane excitonic states. These excitonic states are used to calculate the intraband polarization and terahertz emission of the superlattice system in response to excitation via an ultrashort optical pulse. Our results show that the higher in-plane excitonic states often modify considerably the terahertz emission relative to the results obtained using a $1s$ exciton basis, but that under some excitation conditions a $1s$ exciton basis gives accurate results. Good agreement between experimental and theoretical results is obtained.

DOI: 10.1103/PhysRevB.69.165310 PACS number(s): 78.47.+p, 73.21.Cd, 78.67.Pt, 42.65.Re

I. INTRODUCTION

After the ground-breaking work of Bloch in 1928,[1] there has been a considerable amount of work done on Bloch oscillations (BO's). As discussed by James and co-workers,[2–4] the energy levels of electrons in a periodic potential of period d in the presence of a constant electric field F are given by E_0+meFd, where E_0 is a reference energy, e is the modulus of the charge on an electron, and m is an integer. The energy levels form the so-called Wannier-Stark ladder (WSL) and the eigenstates are localized if Zener tunneling[5] is neglected. BO's result from wave packets formed from the superposition of WSL states. The energy spacing of the WSL, eFd, is usually written in terms of Bloch frequency ω_B as $eFd \equiv \hbar\omega_B$.

The recent intensive interest in BO's and the WSL began after the proposal of the superlattice by Esaki and Tsu in early 1970s.[6] The WSL was first detected by Mendez *et al.* in a biased semiconductor superlattice (BSSL) via photocurrent and photoluminescence measurements.[7] More recently, much interest has shifted from the characterization of the WSL stationary states to the observation the coherent dynamics of carriers excited via ultrashort optical pulses. The most common experimental techniques for observing coherent dynamics in a BSSL are four-wave mixing techniques and the direct detection of the terahertz field generated by the oscillating electronic wave packets.[8–11]

On the theoretical side, there have been a relatively large number of approaches employed to calculate the coherent dynamics in BSSL's. Among these formalisms, the most common approaches are those based on the semiconductor Bloch equations (SBE's),[12–16] and various forms of the dynamics controlled truncation (DCT) theory.[17–20] The SBE's have been used successfully to describe a wide range of experimental results, including the ac Stark effect, Rabi oscillations, and terahertz emission.[13,21,22] In principle, the SBE's are a nonperturbative method and can treat the optical field in infinite order. However, it has been shown that the SBE's within the Hartree-Fock (HF) approximation neglect the crucial electron-hole correlations within an exciton when carried out beyond first order in the optical electric field.[18,23–28] The DCT theory on the other hand can in principle treat all correlations exactly to any desired order in the optical field. It has been employed to calculate the intraband polarization of coupled-double quantum wells and BSSL's to second order.[27,29,30]

Most authors using either SBE's or DCT employ a free electron-hole basis to calculate the coherent dynamics. Such a basis, however, is not often favorable to the numerical calculation of the BSSL system where the electron-hole Coulomb interaction plays an important role as the basis size required is usually very large. Furthermore, it is essentially due to the use of the free electron and hole basis that the crucial correlation between the electron and hole within an exciton is not treated correctly by the SBE's in the Hartree-Fock approximation. Hader *et al.*,[21] by including phonons in their model, have mitigated the problem introduced via the Hartree-Fock approximation. However, this problem is completely removed by employing an exciton basis and using DCT theory. This is the approach used in the present work. This formalism has been successfully applied to the calculation of coherent dynamics up to infinite order in the optical field.[27,30,31]

In previous publications, we have restricted the basis used in dynamics calculations to include only $1s$ excitons.[27,30,31] The justification for this reduced basis is twofold. First, for excitation via optical energies below the zeroth heavy-hole $1s$ exciton transition energy, $\hbar\omega_0$, the absorption is dominated by $1s$ excitons. Second, using the usual methods, the calculation of bound and unbound excitonic states in a BSSL is computationally very time consuming. Although much of the physics can be understood without the higher continuum states, these states have been shown to be important in describing the full absorption spectrum including the Fano resonances.[32] As we shall show here, these states can also play a role in the nonlinear coherent response of a BSSL.

In this work, we first present a method to calculate both the bound and unbound excitonic states in a BSSL. The

method is essentially an extension of the method that Dignam and Sipe[33] developed to calculate the $1s$ exciton states of a BSSL. In order to verify the validity of the method, the calculated excitonic states are first employed to calculate the linear absorption spectra of BSSL's. The method is very efficient, typically requiring less than 800 basis states. There are a number of other authors who have presented accurate methods for the calculation of the absorption spectra of BSSL's. Some of these methods[34] do not explicitly calculate the electronic states of the system, while others[35–39] employ very large numbers of noninteracting basis states typically from 5×10^3 to 10^6. Both of these factors can become a serious limitation in the calculation of the nonlinear coherent dynamics in these systems. It is because we wish to use our basis to calculate the intraband dynamics of BSSL's that we employ the excitonic basis presented in this work.

Using the full excitonic basis that includes both $1s$ and higher in-plane excitonic states (HIES), we find that the intraband polarization and the terahertz emission can be strongly affected by the HIES of the BSSL system. In particular, we find that the HIES can significantly influence the dc component, amplitude and phase of the intraband polarization and the phase and amplitude of the terahertz radiation relative to a $1s$-exciton model. Calculations with the full excitonic basis also show that the previous 1s-exciton-based model for dynamics calculation gives accurate results for excitation where the exciting laser energy is well below the zeroth heavy-hole transition energy. However, when the exciting laser energy approaches and goes above the zeroth heavy-hole $1s$ exciton transition energy $\hbar\omega_0$, the previous $1s$-exciton models do not correctly describe the dynamics of the system.

The theoretically predicted terahertz signal is directly compared to experiment. Here, we present experimental results investigating the THz emission of a BSSL as function of the exciting laser energy. Although other experiments[40,41] have been performed on the terahertz emission from BSSL's, this work focuses on the dependence of the terahertz emission on the spectral position of the exciting laser pulse, while simultaneously retaining precise control of the excitation conditions during the terahertz experiment. We find good agreement of theory with experiment.

The paper is organized as follows. First, a method of obtaining the excitonic stationary states of a BSSL system is given in Sec. II A. In Sec. II B, the absorption spectrum is calculated with the full excitonic basis and compared with existing experimental results. In Sec. III A, we present the theory used to calculate the intraband polarization and the terahertz emission. In Sec. III B, we compare the results using a full excitonic basis with those using a $1s$-exciton basis. In Sec. III C, we compare our theoretical results for terahertz radiation with our experimental results. Finally, in Sec. IV, a summary is presented.

II. STATIONARY EXCITONIC STATES

A. Theory

In this section, we present a tight-binding approach for calculating all the optically active bound and unbound excitonic states of a BSSL. This means that we calculate only the states with in-plane s symmetry and with a center-of-mass wave vector $\mathbf{K}$ that is zero. For a type-I superlattice, the envelope-function Hamiltonian in the presence of a static electric field may be written as[33]

$$H_0(r,z_e,z_h)=H_0'(r,z_e,z_h)+U^e(z_e)+U^h(z_h)+eFz, \tag{2.1}$$

where H_0', which contains the kinetic and Coulomb energy terms, is given by

$$H_0'(r,z_e,z_h)=\frac{-\hbar^2}{2\mu(z_e,z_h)}\frac{1}{r}\frac{\partial}{\partial r}\left(r\frac{\partial}{\partial r}\right)-\frac{\hbar^2}{2}\frac{\partial}{\partial z_e}\frac{1}{m_{ez}^*}\frac{\partial}{\partial z_e}$$
$$-\frac{\hbar^2}{2}\frac{\partial}{\partial z_h}\frac{1}{m_{hz}^*}\frac{\partial}{\partial z_h}-\frac{e^2}{\epsilon\sqrt{r^2+z^2}}. \tag{2.2}$$

In Eq. (2.2), z_e and z_h denote the z coordinates of the electron and hole, respectively, $z\equiv z_e-z_h$, and r denotes the electron-hole separation in the xy (transverse) plane. The layer-dependent, transverse, reduced effective mass is defined by $\mu^{-1}(z_e,z_h)\equiv m_{e\|}^*(z_e)^{-1}+m_{h\|}^*(z_h)^{-1}$, where $m_{e\|}^*(z_e)$ $[m_{h\|}^*(z_h)]$ is the transverse electron (hole) mass. The layer-dependent effective mass for the electron (hole) in the z direction is denoted by $m_{ez}^*(z_e)$ $[m_{hz}^*(z_h)]$. The average dielectric constant of the structure is given by ϵ. Since only the optically accessible s-symmetry states will be considered in this work, the angular dependence in the Hamiltonian in Eq. (2.2) has been omitted. Finally, in Eq. (2.1), $U_\sigma(z_\sigma)$ $\{\sigma\in[e,h]\}$ is the superlattice potential for the electron (hole) and is described by

$$U_\sigma(z_\sigma)=V_\sigma\left[1-\sum_j R(L{:}z_\sigma-jd)\right], \tag{2.3}$$

where V_σ is the electron or hole well depth and j is an integer. The function $R(L{:}z)$ is a rectangle function of height 1 and width L centered on $z=0$, where L is the width of the quantum wells.

The exciton Hamiltonian of Eq. (2.1) is invariant under a translation of the exciton center of mass by a distance of md, where m is an integer.[33] The translational symmetry in the BSSL's indicates that the exciton envelope function has a form similar to the usual Bloch wave function. Thus the periodicity in the reciprocal lattice allows one to write the exciton envelope function in the Wannier representation:

$$\psi_\mu^{K_z}(r,z_e,z_h)$$
$$=\frac{1}{\sqrt{2N+1}}\sum_{m=-N}^{N}W_\mu(r,z_e-md,z_h-md)e^{iK_zmd}, \tag{2.4}$$

where μ is the internal quantum number of an exciton, K_z is the exciton center-of-mass wave number in the z direction, and $2N+1$ is the number of periods in the superlattice. The $W_\mu(r,z_e,z_h)$ are the exciton Wannier functions.[33] The z-component center-of-mass wave vector K_z will be set to zero hereafter due to the negligible momentum of exciting photons.

The problem is now reduced to calculating the exciton Wannier function $W_\mu(r,z_e,z_h)$. We expand the $W_\mu(r,z_e,z_h)$ in a basis composed of the eigenstates of various two-well Hamiltonians.[33] A two-well Hamiltonian H_j^{TW} is a Hamiltonian for an *interacting* electron and hole where the electron is in a well centered at $z_e=jd$ and the hole at $z_h=0$. The jth two-well Hamiltonian is given by

$$H_j^{TW}(z_e,z_h,r)=H_0'+V_e[1-R(L;z_e-jd)]+V_h[1-R(L;z_h)], \tag{2.5}$$

where H_0' is defined in Eq. (2.2).

In the previous work[33] where only the $1s$ excitons were considered, the eigenstates of the two-well Hamiltonian were solved variationally through a $1s$-like variational wave function. In this work, however, all the s-symmetry excitonic states in the plane are calculated. Therefore, apart from the first index j for describing the electron-hole separation of the given two-well Hamiltonian H_j^{TW}, a second index β is required to label the different eigenstates of H_j^{TW}. The quantum number β describes the $1s$, $2s$, $3s$, . . . (up to the continuum) s-symmetry states of in-plane motion. We define the eigenstates of the two-well Hamiltonian H_j^{TW} by $\Phi_{j\beta}(r,z_e,z_h)$. We solve for the two-well eigenstates by expanding them in an appropriate basis. We begin by rewriting the two-well Hamiltonian, Eq. (2.5), as follows:

$$\begin{aligned}H_j^{TW}&=\left[\frac{-\hbar^2}{2\mu(z_e,z_h)}\frac{1}{r}\frac{\partial}{\partial r}\left(r\frac{\partial}{\partial r}\right)\right]+\left\{-\frac{\hbar^2}{2}\frac{\partial}{\partial z_e}\frac{1}{m_{ez}^*}\frac{\partial}{\partial z_e}+V_e[1-R(L;z_e-jd)]\right\}+\left\{-\frac{\hbar^2}{2}\frac{\partial}{\partial z_h}\frac{1}{m_{hz}^*}\frac{\partial}{\partial z_h}+V_h[1-R(L;z_h)]\right\}-\frac{e^2}{\epsilon\sqrt{r^2+z^2}}\\&\equiv H_\parallel+H_e^j+H_h^0-\frac{e^2}{\epsilon\sqrt{r^2+z^2}}.\end{aligned} \tag{2.6}$$

For simplicity we neglect the field dependence of the two-well potentials in Eq. (2.6). This approximation can be shown to be a good one as long as the width of quantum well is not too shallow and the applied dc field is not too large. For the system considered in this paper, the field dependence of the two-well Hamiltonian has a negligible influence.[33]

The basis used to determine the eigenstates of the two-well Hamiltonian are the eigenstates of $H_\parallel+H_e^j+H_h^0$, which can be written as

$$\phi_k(r,z_e-jd,z_h)=f_e^m(z_e-jd)f_h^n(z_h)g_k(r), \tag{2.7}$$

where $f_e^m(z_e-jd)$ ($f_h^n(z_h)$) is the mth (nth) eigenstate of the Hamiltonian H_e^j (H_h^0) and $g_k(r)$ is the kth eigenstate of $H_\parallel$, which is independent of j. As has been shown previously,[43] when the well width is about 10 nm or less (which is the case for the BSSL's considered here), we need only include the $m=n=1$ along-axis states, which we now denote simply by $f_\sigma(z_\sigma)$ for $\sigma\in\{e,h\}$.

The $g_k(r)$ satisfies the eigenvalue equation

$$\frac{-\hbar^2}{2\bar{\mu}}\frac{1}{r}\frac{\partial}{\partial r}\left(r\frac{\partial}{\partial r}\right)g_k(r)=E_k^\parallel g_k(r), \tag{2.8}$$

where $\bar{\mu}$ is the appropriate average of $\mu(z_e,z_h)$. To quantize the energies, we impose the boundary condition $g_k(R)=0$, where R is a large radius to be defined later. Thus, the solutions are Bessel functions of the first kind of order 0,

$$g_k(r)=N_kJ_0(kr), \tag{2.9}$$

where the N_k are normalization constants given by

$$N_k=\frac{\sqrt{2}}{R|J_1(kR)|}, \tag{2.10}$$

and the energies are given by $E_k^\parallel=\hbar^2k^2/2\bar{\mu}$. The boundary condition $g_k(R)=0$ yields $J_0(kR)=0$, which determines k. The choice of R in actual calculations is dictated by a balance between achieving very accurate energies and wave functions for the low-energy states ($1s$,$2s$, . . .) while still giving accurate density of states at high energies and keeping the basis at a manageable size. In practice, we find that $R=40a_0$ gives very accurate exciton states up to the $4s$ state and yields converged results for both absorption and polarization calculations for the excitation energies of interest.[42] Here a_0 is the exciton Bohr radius which is roughly 15 nm for GaAs. Now, with the basis states in Eq. (2.7), the eigenstates of the two-well Hamiltonian [Eq. (2.5) or (2.6)] are expanded as

$$\Phi_{j\beta}(r,z_e,z_h)=\sum_k A_k^{j\beta}N_kf_e(z_e-jd)f_h(z_h)J_0(kr), \tag{2.11}$$

where $A_k^{j\beta}$ are the expansion coefficients. The coefficients $A_k^{j\beta}$, and hence the eigenstates $\Phi_{j\beta}(r,z_e,z_h)$, are determined by diagonalizing the two-well Hamiltonian in Eq. (2.6) in this orthogonal basis. For convergence, the number of $J_0(kr)$ (k states) required for a given j needs to be 400 for $R=40a_0$. The most computationally intensive part of this calculation is the evaluation of the Coulomb matrix elements. In Appendix A, we present a very efficient way to evaluate these matrix elements.

Once the eigenstates $\Phi_{j\beta}(r,z_e,z_h)$ of the two-well Hamiltonian have been calculated, the eigenstates of the BSSL can be obtained by expanding the exciton Wannier functions in the basis of these two-well eigenstates. Thus the general exciton envelope function in Eq. (2.4) is written as

$$\psi_\mu(r,z_e,z_h)=\frac{1}{\sqrt{2N+1}}\sum_{m=-N}^{N} W_\mu(r,z_e-md,z_h-md)$$

$$=\frac{1}{\sqrt{2N+1}}\sum_{m=-N}^{N}\sum_{j=-N}^{N}\sum_{\beta=1}^{M} C_{j\beta}^{\mu} \times\Phi_{j\beta}(r,z_e-jd-md,z_h-md), \qquad (2.12)$$

where $C_{j\beta}^{\mu}$ are expansion coefficients and M is the highest in-plane state included in the calculation. It is important to note that although the number of k states needed to expand a two-well state is 400, the number of in-plane excitonic states, M, for a given j, needed in Eq. (2.12) is much less than this. Typically, we find that $M=60$ is enough for convergence. The required number of quantum wells, $2N+1$, is 13–31, depending on the applied field strength.

Using the exciton envelope functions $\psi_\mu(r,z_e,z_h)$ in Eq. (2.12), the eigenvalue equation is

$$\sum_{j=-N}^{N}\sum_{\beta=1}^{M}(H_0)_{ij}^{\alpha\beta}C_{j\beta}^{\mu}=E_\mu\sum_{j=-N}^{N}\sum_{\beta=1}^{M}C_{j\beta}^{\mu}O_{ij}^{\alpha\beta}, \qquad (2.13)$$

where

$$(H_0)_{ij}^{\alpha\beta}\equiv\sum_{m=-N}^{N}\langle\Phi_{i\alpha}^{m}|H_0|\Phi_{j\beta}^{0}\rangle \qquad (2.14)$$

and

$$O_{ij}^{\alpha\beta}=\sum_{m=-N}^{N}\langle\Phi_{i\alpha}^{m}|\Phi_{j\beta}^{0}\rangle, \qquad (2.15)$$

where the ket $|\Phi_{j\sigma}^{m}\rangle$ is defined by

$$\langle r,z_e,z_h|\Phi_{j\beta}^{m}\rangle=\Phi_{j\beta}(r,z_e-jd-md,z_h-md). \qquad (2.16)$$

Explicit expressions for $(H_0)_{ij}^{\alpha\beta}$ are given in Appendix B. The two-well eigenstates $\Phi_{j\beta}(r,z_e,z_h)$ are not orthogonal. Therefore, it is necessary to solve the generalized eigenvalue equations as in Eq. (2.13) to obtain the expansion coefficients $C_{j\beta}^{\mu}$.

It is worth pointing out a number of features of our approach. First, for a given structure, the two-well eigenstates need only be calculated once. They can then be used for any dc field strength of interest. Second, the final basis used in Eqs. (2.12) and (2.13) is of size $M(2N+1)=60\times13\rightarrow60\times31$.

B. Absorption

In this section, we use our excitonic states to calculate the absorption spectra of a BSSL for different static electric fields and compare to experimental results. The field-dependent excitonic absorption per unit volume, $\alpha(\omega)$, is given by

$$\alpha(\omega)=\sum_{\mu}\frac{4\pi e^2|\xi\cdot\mathbf{p}_{cv}|^2}{\omega m_0^2 n' c}\alpha_\mu\delta[E_\mu-\hbar\omega], \qquad (2.17)$$

where ξ is the electric-field polarization vector, $\mathbf{p}_{cv}$ is the momentum matrix element between the bulk conduction-band and valence-band Bloch states at the band edges, m_0 is the free electron mass, n' is the refractive index of the medium, and α_μ is the absorption strength given by[43]

$$\alpha_\mu=\frac{1}{d}\left|\int dz W_\mu(r=0,z,z)\right|^2. \qquad (2.18)$$

The system we investigate here is a GaAs/$Ga_{0.3}Al_{0.7}As$ superlattice with well width of 6.7 nm and barrier width of 1.7 nm. The physical parameters used are given in Ref. 43. We begin by examining the influence of the HIES on the

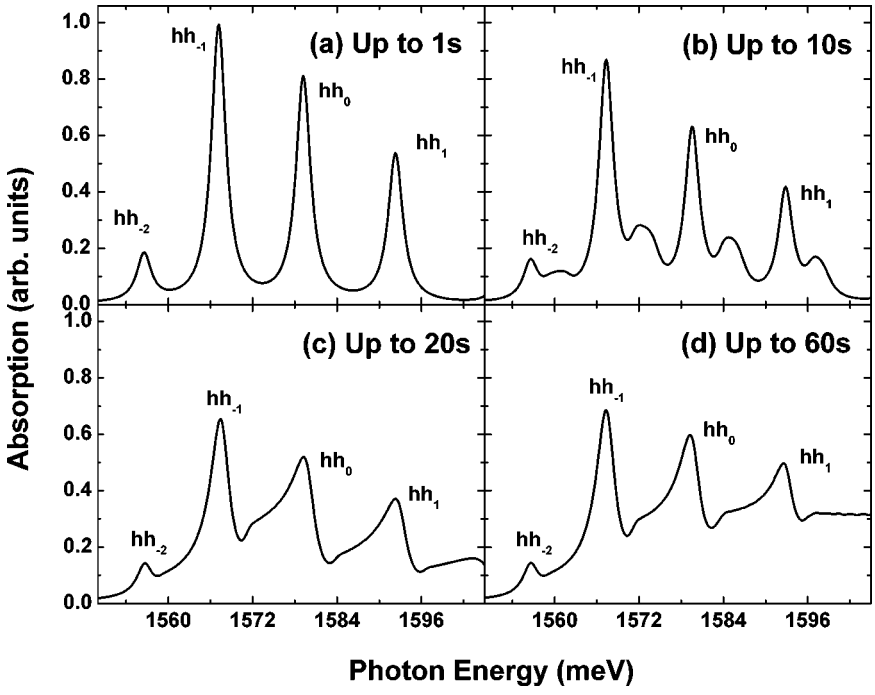

FIG. 1. The calculated absorption spectra of the 67/17 superlattice under a bias of 15 kV/cm with the inclusion of a different number of higher in-plane excitonic states, as indicated.

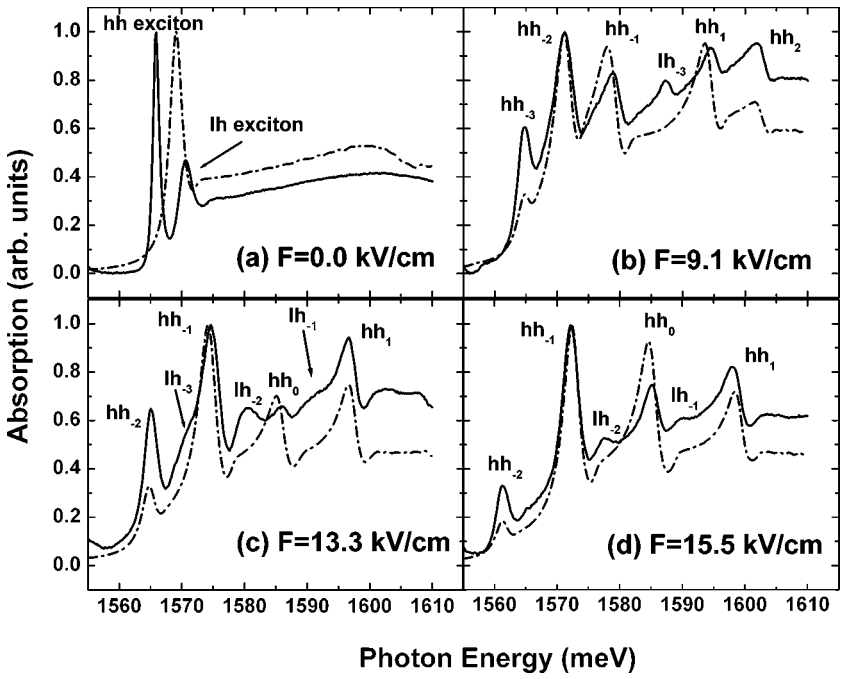

FIG. 2. The comparison of the calculated absorption spectra (dashed line) with the experimental spectra (solid line) of Holfeld *et al.* (Ref. 44) for the 67/17 superlattice for different dc electric fields F.

absorption spectrum for $F=15$ kV/cm. Four optical absorption spectra with the inclusion of different number of HIES are shown in Fig. 1. As is discussed in Appendix C, we can label the $1s$ states by an excitonic WSL index n, such that the intraband dipole of the state is given approximately by end. The peaks associated with heavy-hole excitons with excitonic WSL index n are labeled by hh_n in the figure. In Fig. 1(a), only $1s$ excitons are included in the basis. In Figs. 1(b–d), HIES up to $10s$, $20s$, and $60s$, respectively, are included. Not surprisingly, the absorption spectra are greatly affected by the HIES, especially for $\hbar\omega > 1570$ meV. We find that convergence is reached for $\hbar\omega < 1650$ meV when $M=60$ and $N=6$. We also note that the results obtained with $R=30a_0$ and $R=40a_0$ are identical over this frequency range, indicating that a radius of $R=40a_0$ is sufficient. An intuitive schematic way that explains the convergence of both absorption and dynamics calculations is discussed in Appendix C.

Figure 2 shows the comparison of the converged absorption spectra under various applied external dc electric-field strengths along with the corresponding experimental results of Holfeld *et al.*,[44] who measured the transmission spectra of a $GaAs/Ga_{0.3}Al_{0.7}As$ (6.7/1.7) nm superlattice with a halogen lamp at a temperature of 10 K. In the figure, lh_n denotes the light-hole absorption peaks. The experimental spectra were corrected for the spectral response of the system and spectral modulations due to Fabry-Perot interferences. In the calculation, a full width at half maximum (FWHM) of 2.5 meV has been used. The calculated results have been scaled such that the dominant peak is of the same height as the corresponding experimental peak. The agreement is in general very good, with the calculations reproducing the peak energies and the clear signatures of the Fano resonances arising from the mixing of the $1s$ excitonic states and the continuum states of lower WSL states.[32] The main differences are due to the neglect of the light holes in our calculations. Thus some peaks in the experiments are not seen in the calculations. For example, the light-hole peaks at 1.569 eV in Fig. 2(a), 1.587 eV in Fig. 2(b), and 1.581 eV in Fig. 2(c), respectively, are not seen in the theoretical simulations. The obvious discrepancy in the main peak position in the $F=0$ kV/cm case in Fig. 2(a) may due to the light-hole and heavy-hole mixing that is not included in our simulation.

The agreement of the absorption spectra with the calculated results indicates that the calculated excitonic eigenstates form a very good basis for dynamic calculations. In the following section, this full excitonic basis is employed in the calculation of the coherent intraband response of the BSSL system to ultrashort optical pulse excitation.

III. DYNAMICS

A. Theory

To calculate the intraband polarization and terahertz emission from a BSSL system excited by an ultrashort optical pulse, the dynamic equations to second order in the optical field are required. The dynamic equations employed in this work are similar to those we have presented in previous work[27,30] except that a full excitonic basis is employed, rather than just the $1s$-exciton states. Consequently, the number of differential equations is at least three orders of magnitude larger than the $1s$-exciton case. This considerably increases the calculation burden and requires an efficient basis.

Because we want the polarization to second order in the optical field, exciton-exciton interactions and phase-space filling effects can rigorously be neglected.[30] The Hamiltonian of the superlattice excitons in the presence of dc, ac, and optical (OP) electric fields is thus given by

$$H(t)=H_0+H_{ac}(t)+H_{OP}(t), \tag{3.1}$$

where H_0 is the exciton-envelope-function Hamiltonian as defined in Eq. (2.1) and its second quantized form is given by

$$H_0 = \sum_{\mu} E_{\mu} B_{\mu}^{\dagger} B_{\mu}, \tag{3.2}$$

where $B_{\mu}^{\dagger}$ (B_{μ}) is the creation (annihilation) operator for the exciton in state $|\psi_{\mu}\rangle$ with internal quantum number μ and energy E_{μ}. The term

$$H_{ac}(t) \equiv -V\mathbf{E}_{ac}(t) \cdot \mathbf{P}_{intra} \tag{3.3}$$

is the interaction Hamiltonian between the terahertz ac field $\mathbf{E}_{ac}(t)$ and the excitons, where $\mathbf{P}_{intra}$ is the intraband polarization operator defined by

$$\mathbf{P}_{intra} = \frac{1}{V} \sum_{\mu\mu'} \mathbf{G}_{\mu\mu'} B_{\mu}^{\dagger} B_{\mu'}. \tag{3.4}$$

In this expression, $\mathbf{G}_{\mu\mu'}$ is the intraband dipole matrix element between two excitonic states $|\psi^{\mu}\rangle$ and $|\psi^{\mu'}\rangle$, and is given by

$$\mathbf{G}_{\mu\mu'} = \langle \psi^{\mu}| -e(z_e - z_h)|\psi^{\mu'}\rangle. \tag{3.5}$$

Finally, the last term in $H(t)$ is

$$H_{op}(t) \equiv -V\mathbf{E}_{op}(t) \cdot \mathbf{P}_{inter}, \tag{3.6}$$

which is the interaction Hamiltonian between the optical field $\mathbf{E}_{op}(t)$ and the excitons, where $\mathbf{P}_{inter}$ is the interband polarization operator defined by

$$\mathbf{P}_{inter} = \frac{1}{V} \sum_{\mu} [\mathbf{M}_{\mu} B_{\mu}^{\dagger} + \mathbf{M}_{\mu}^{*} B_{\mu}]. \tag{3.7}$$

The interband dipole matrix element of the μth excitonic state is given by

$$\mathbf{M}_{\mu} = \mathbf{M}_0 \sqrt{A} \int dz\, \psi^{\mu *}(z,z,0), \tag{3.8}$$

where $\mathbf{M}_0$ is the bulk interband dipole matrix element and A is the transverse area. The derivations of the general forms of the interband and the intraband dipole matrix elements are given in Ref. 30. The explicit forms of the interband and intraband dipole matrix elements are presented in Appendix D.

From the exciton Hamiltonian, it is straightforward to obtain the dynamic equations from the Heisenberg equation of motion. To second order in the optical field, these equations are[27]

$$i\hbar \frac{d\langle B_{\mu}^{\dagger}\rangle}{dt} = -\left(E_{\mu} + \frac{i\hbar}{T_{2inter}}\right)\langle B_{\mu}^{\dagger}\rangle + \mathbf{E}_{opt}(t) \cdot \mathbf{M}_{\mu}^{*} + \mathbf{E}_{ac}(t) \cdot \sum_{l} \mathbf{G}_{l\mu} \langle B_{l}^{\dagger}\rangle, \tag{3.9}$$

$$i\hbar \frac{d\langle B_{\mu}^{\dagger} B_{\mu'}\rangle}{dt} = \left(E_{\mu'} - E_{\mu} - \frac{i\hbar}{T_{\mu\mu'}}\right)\langle B_{\mu}^{\dagger} B_{\mu'}\rangle + \mathbf{E}_{opt}(t) \cdot [\mathbf{M}_{\mu}^{*}\langle B_{\mu'}\rangle - \mathbf{M}_{\mu'}\langle B_{\mu}^{\dagger}\rangle] + \mathbf{E}_{ac}(t) \cdot \sum_{l} [\mathbf{G}_{l\mu}^{*}\langle B_{l}^{\dagger} B_{\mu'}\rangle - \mathbf{G}_{\mu' l}\langle B_{\mu}^{\dagger} B_{l}\rangle], \tag{3.10}$$

where T_{2inter} is the interband dephasing time, and $T_{\mu\mu'}$ is defined such that $T_{\mu\mu'} = T_1$ (excitonic population decay time) if $\mu = \mu'$, and $T_{\mu\mu'} = T_{2intra}$ if $\mu \neq \mu'$, where T_{2intra} is the intraband dephasing time. To focus on the influence of the HIES, the external terahertz ac field $\mathbf{E}_{ac}(t)$ is not included in this work. The optical field considered here is an ultrashort Gaussian optical pulse ($\sim$75 fs FWHM) with central frequency ω_c and duration τ_p, which takes the form

$$\mathbf{E}_{opt} = \mathbf{A}_0 e^{-(t/\tau_p)^2} e^{-i\omega_c t} + \text{c.c.} \tag{3.11}$$

By solving a system of equations given by Eqs. (3.9) and (3.10), the time-dependent reduced density matrix elements $\langle B_{\mu}^{\dagger} B_{\mu'}\rangle$ are obtained. These are then used to calculate the intraband polarization as given by the expectation value of Eq. (3.4). We can calculate the terahertz field by taking the second derivative of intraband polarization with respect to time. The issue of the number of HIES to achieve convergence in dynamics calculations is discussed in Appendix C.

B. Theoretical results

In this section we present the calculated intraband dynamics. The superlattice that was introduced in Sec. II B is used for dynamics calculations in this section. The external dc electric field is taken to be 12.5 kV/cm. The FWHM of the laser pulse is 75 fs. The dephasing time constants for the interband and intraband polarizations are taken, respectively, to be 0.33 ps and 0.5 ps. The population decay constant T_1 is taken to be infinite as it is expected to be much longer than the dephasing times. As already mentioned in the preceding section, converged results can be obtained for the inclusion of the HIES up to 60 s. Therefore, all the dynamics calculations below are made by including all the in-plane states up to 60 s.

In Fig. 3, we present the intraband polarization, calculated with the 1s exciton basis and with the full excitonic basis for different laser energies given by $\hbar\omega_c = \hbar\omega_0 + \theta\hbar\omega_B$, where $\theta = -2.7, -1.1, 1.4, 2.3$. We choose these θ values to allow direct comparison with the experimental results in Sec. C. The polarization is normalized to the exciton population in all that follows, and so is effectively the polarization per exciton. We begin with a discussion of the results calculated with the 1s basis. In this case, when $\theta < 0$ ($\theta > 0$), the excitons created have WSL indices $n < 0$ ($n > 0$). Thus, they have permanent intraband dipole moments that are positive (negative). Therefore, as θ is increased from -2.7 to 2.3, the dc component of the intraband dipole moment changes from positive to negative, as seen in Fig. 3. In addition, as has been discussed in previous works,[45,46] when $\theta < 0$, a Gauss-

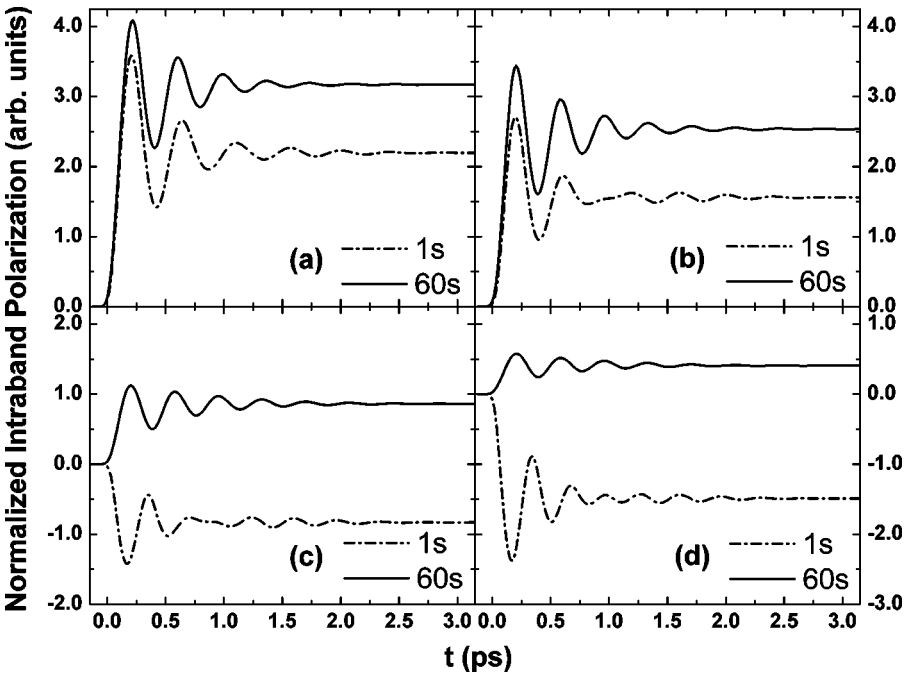

FIG. 3. The calculated intraband polarizations of the 67/17 superlattice with $F=12.5$ kV/cm excited by laser pulses with central energies:
(a) $E_c=\hbar\omega_0-2.7\hbar\omega_B$,
(b) $E_c=\hbar\omega_0-1.1\hbar\omega_B$,
(c) $E_c=\hbar\omega_0+1.4\hbar\omega_B$, and
(d) $E_c=\hbar\omega_0+2.3\hbar\omega_B$.

ian optical pulse creates a wave packet with a centroid that initially moves in the $-z$ direction, thereby resulting in an intraband polarization that oscillates roughly as $\sin(\omega_B t)$. Conversely, when $\theta<0$, the resulting intraband polarization phase differs by π and oscillates roughly as $-\sin(\omega_B t)$. This feature is also exhibited in Fig. 3, where the phase change in the oscillations is observed to occur near $\theta=0$.

We now consider the results obtained when the HIES are included (full calculation). When $\theta<0$, both the $1s$ states and all of the HIES that are optically created have WSL indices n that are less than zero. Thus, we expect the dc component and phase of the oscillations to be similar to that found in the $1s$ calculation. Therefore, in Fig. 3, we see that for $\theta=-2.7,-1.1$, the intraband polarization is not greatly affected by the HIES. The main differences between the $1s$ and full calculations are an increase in the dc component of the polarization and a small increase in the oscillation frequency for the full calculation. The increase in dc component is due to the fact that the HIES created by the optical pulse will have a WSL index n, which is larger in magnitude than that for the $1s$ excitons (see Fig. 6 in Appendix C), thereby leading to an increased permanent dipole moment. The increase in the oscillation frequency arises because the energy separation between $1s$ WSL excitonic states is less than that of the more weakly bound HIES when $n<0$.[27] Thus, the BO frequency of the HIES is higher than that of the $1s$ excitons. The net result of the HIES is to give a slight increase in the BO frequency, as observed.

Now, as θ is increased, the laser will excite more and more HIES (see Fig. 6 in Appendix C). If $\theta>0$, then although many $1s$ excitons with $n>0$ will be created, most of the HIES created will still have $n<0$. Therefore, the portion of the intraband polarization due to the HIES will have a dc component and a phase that is the negative of that due to the $1s$ states. This results in a canceling-out of the effects of the $n>0$ $1s$ excitonic states by the HIES. It turns out that the HIES along with the $n<0$ $1s$ states dominate the intraband polarization for $\theta>0$. As is seen in Figs. 3(c) and 3(d), the net result is that there is no change in the sign of the dc component of the polarization or in the phase of the oscillations when θ becomes positive. Thus, for lasers in this frequency range, there is a large difference between the $1s$ and full calculations. The above physical picture also explains the large decrease in oscillation amplitude when the HIES are included; because the polarization from the HIES is π out of phase with the $1s$ exciton polarization in this case, the two contributions destructively interfere, resulting in a small net polarization amplitude. Finally, the *decrease* in the oscillation frequency when the HIES are included arises because the energy separation between $1s$ WSL excitonic states is *greater* than that of the more weakly bound HIES when $n>0$.[27] This yields a BO frequency for the HIES that is lower than that of the $1s$ excitons. The net result of the HIES is to give a slight decrease in the BO frequency, as observed in Fig. 3(d) [or Fig. 4(d)].

By taking the second derivative of the intraband polarization with respect to time, one can obtain the far-field terahertz emission signals. The terahertz signals in Fig. 4 correspond to the intraband polarizations in Fig. 3 under the same laser excitation conditions. Again, the results are normalized to population density. We note that any change in the dc component in the intraband polarizations due to the HIES does not affect the terahertz signals appreciably. As can be seen in Figs. 4(a) and 4(b), the terahertz signals calculated by $1s$-exciton and full excitonic basis are essentially the same when the exciting laser energy is well below $\hbar\omega_0$ ($\theta<0$). This is, however, not true when the laser energy is above $\hbar\omega_0$. In particular for the $\theta=2.3$ case, both phase and amplitude of the terahertz signals obtained using the different basis are very different. The reasons for these changes are explained above in the discussion of the intraband polarization. Thus, for the terahertz emission calculations where the

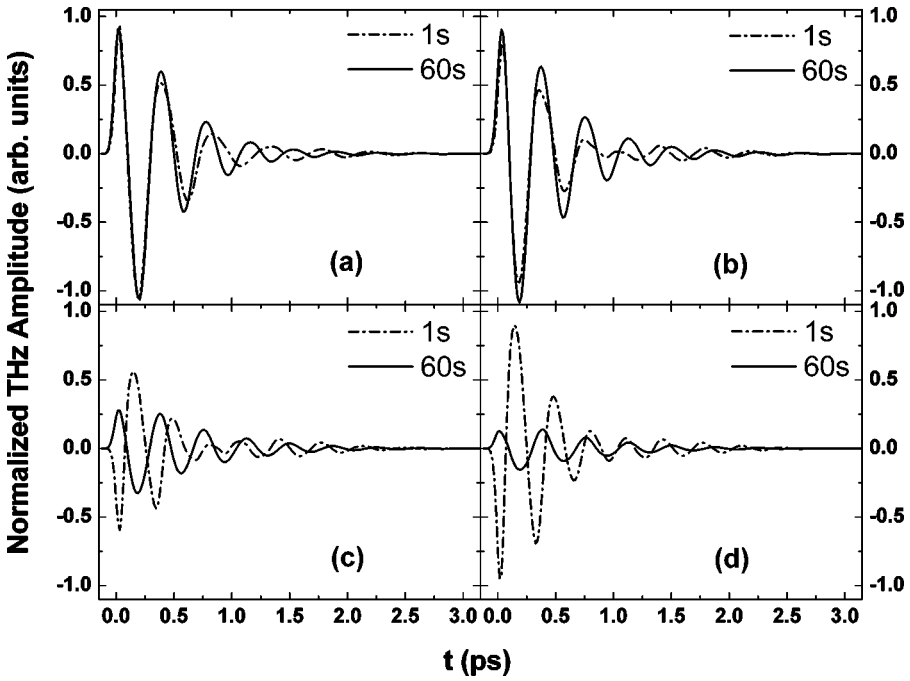

FIG. 4. The calculated terahertz field of the 67/17 superlattice with $F=12.5$ kV/cm excited by laser pulses with central energies:
(a) $E_c=\hbar\omega_0-2.7\hbar\omega_B$,
(b) $E_c=\hbar\omega_0-1.1\hbar\omega_B$,
(c) $E_c=\hbar\omega_0+1.4\hbar\omega_B$, and
(d) $E_c=\hbar\omega_0+2.3\hbar\omega_B$.
The field is normalized by the carrier density.

exciting laser energy is below $\hbar\omega_0$, the model based on the full excitonic basis can be replaced by the $1s$-exciton model as has been done in a number of recent papers.[27,30] This is important, as the method based on $1s$ excitons is at least 10^4 times more efficient. However, for the terahertz emission calculations with laser energy approaching and above $\hbar\omega_0$, a full excitonic basis would be required for a more realistic description.

C. Experimental results

We now turn to our experimental results for the terahertz emission from a $GaAs/Al_{0.3}Ga_{0.7}As$ (6.7/1.7) nm superlattice. To apply an electric field, a semitransparent Cr/Au Schottky contact was evaporated on top of the structure. On the substrate side an ohmic contact was formed by evaporating and annealing a ZnAu alloy film. The substrate was partially removed by wet etching to allow for measuring in transmission geometry. The emitted terahertz was detected with the help of the free-space electro-optic (EO) sampling technique, introduced by Wu and Zhang.[47] The emitted terahertz radiation was collected and imaged by two pairs of off-axis parabolic mirrors. The first pair produces a terahertz focus at which position a chopper wheel was placed, modulating the terahertz signal, to support detection by a lock-in amplifier. The second pair of parabolic mirrors focused the terahertz radiation onto a 200 μm thick, $\langle 110\rangle$ ZnTe crystal used as EO detector. The birefringence induced in the ZnTe crystal by the terahertz electric field was sampled by a gate pulse copropagating along the terahertz beam path. The polarization change of the gate beam is then analyzed by a shot-noise limited detection scheme.[48] The detected terahertz signal was corrected by the response function of the ZnTe detector according to Leitenstorfer *et al.*[49] Since the detector has a sharp cutoff at around 4 THz, all higher frequencies were omitted. Pump and gate beam were retrieved from a standard Ti:sapphire laser system providing pulses at a repetition rate of 80 MHz. The setup was purged with nitrogen to prevent absorption by water vapor. The sample, tilted by an angle of 50° relative to the exciting beam, was held in a cryostat at $T=10$ K. With a spot diameter of about 600 μm (FWHM), the excitation density was below 10^9 cm^{-2} and kept constant for all measurements by ensuring a constant photocurrent across the sample.

The central energy of the exciting pump pulse with a constant spectral width of 25 meV (FWHM) was shifted through the WSL spectrum for a constant internal field of $F=12.5$ kV/cm. To monitor the excitation conditions, for each experiment, we measured the transmission spectrum of the pump beam, which was reflected off the terahertz beam path by a pellicle beamsplitter. Figure 5 shows the terahertz transients measured for different spectral positions of the pump laser with $\theta=-2.7,-1.1,1.4,2.3$. From experiment, the exact zero-time delay cannot be determined. Therefore, the traces were shifted manually to an artificial $t=0$. In general, theory (Fig. 4) and experiment compare well. The main difference is visible in the amplitude of the first cycle which is smaller in experiment in all cases. The source of the discrepancy is probably due to the limited bandwidth of the detector. It is well known that the creation of polarized electron-hole pairs via the excitation by a short laser pulse will lead to a broadband, single-cycle, terahertz emission.[51] This mechanism contributes to the first cycle of the signal. Since the detection cuts off all frequency components higher than 4 THz, it will lead to a decreased amplitude.

As predicted from theory (solid lines in Fig. 4), the amplitude of the signal stays almost the same when we move from $\theta=-2.7$ to $\theta=-1.1$, but it decreases strongly when we move to $\theta=1.4$ or $\theta=2.3$. The decrease in amplitude is somewhat larger in theory, which could be due to the larger oscillator strength of the direct WSL transition ($n=0$) pre-

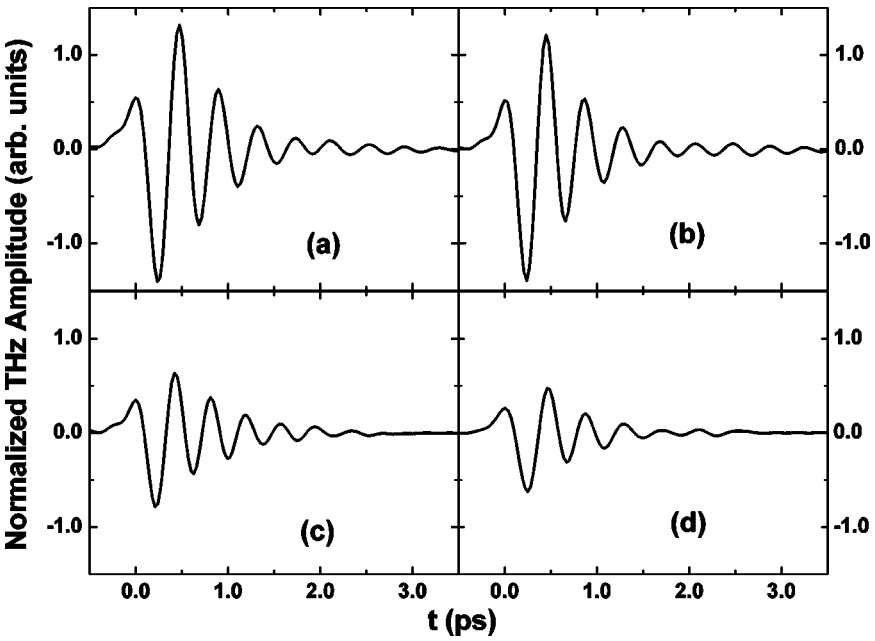

FIG. 5. The experimentally measured terahertz field of a 67/17 superlattice with $F=12.5$ kV/cm excited by laser pulses with the same central energies as in Fig. 4:
(a) $E_c=\hbar\omega_0-2.7\hbar\omega_B$,
(b) $E_c=\hbar\omega_0-1.1\hbar\omega_B$,
(c) $E_c=\hbar\omega_0+1.4\hbar\omega_B$, and
(d) $E_c=\hbar\omega_0+2.3\hbar\omega_B$.
The total carrier density is the same in all cases.

dicted by our model (Fig. 2). Second, as predicted by theory, there is no phase shift observed in experiment when the laser energy passes the WSL center. As discussed above, this shows, that for excitation with $\theta>0$, the wave packet of the HIES associated with bound excitonic states with negative WSL index dominates the intraband dynamics by overcompensating the intraband dipole of the wave packet composed of all excitonic states with $n>0$, inducing the clear discrepancy with the $1s$ exciton model. Martini *et al.*[50] already found in their work an indication of the importance of the excitonic in-plane continuum states on the intraband dynamics of BSSL's. However, the results of this work directly prove that the HIES can play a decisive role.

IV. CONCLUSIONS

We have presented theoretical and experimental results for the terahertz emission of biased semiconductor superlattices excited by ultrashort optical pulses. The theoretical model employed an efficient excitonic basis to calculate the intraband polarization and terahertz field. We found good agreement between the theoretical and experimental results regarding the dependence of the terahertz phase and amplitude on the central laser frequency. We have shown that the inclusion of excitonic states with high in-plane energy can considerably influence the dc component, amplitude, and the phase of the intraband polarization and hence the terahertz emission of the BSSL system. The effect of HIES is especially large when the exciting laser energy is close to or above the zeroth heavy-hole transition energy $\hbar\omega_0$. However, when the laser energy is well below $\hbar\omega_0$, the $1s$ model gives similar results for terahertz emission to those obtained by the full excitonic basis.

One of the key advantages of our theoretical approach is the efficiency of the basis, which makes it possible to consider higher-order nonlinearities. Thus, in future work we plan to use this basis to calculate degenerate four-wave mixing and nonlinear Bloch oscillations.

ACKNOWLEDGMENTS

We would like to thank Margaret Hawton for valuable discussions. This work was supported in part by PREA and the Natural Sciences and Engineering Research Council of Canada. We also acknowledge the financial support by Deutsche Forschungsgemeinschaft (Grants Nos. Ko 686/6, Le 747/11, and the Leibniz Preis).

APPENDIX A: IN-PLANE COULOMB MATRIX ELEMENTS

In the calculation of the matrix elements of the two-well Hamiltonian of Eq. (2.6) in the basis of Eq. (2.11), the evaluation of the kinetic energy is trivial, as the $g_k(r)$ are eigenstates of the in-plane kinetic portion of the two-well Hamiltonian. However, the calculation of Coulomb matrix elements can be time consuming. Thus it is worth the effort to use as efficient a method as possible.

With the usual assumption that $g_k(r)$ varies slowly over a unit cell, the Coulomb contribution due to in-plane motion, $V_{kk'}$, takes the form

$$V_{kk'}=\int_{-\infty}^{\infty}dz_e f_e^2(z_e)\int_{-\infty}^{\infty}dz_h f_h^2(z_h)\int_0^R dr\cdot r g_k(r)g_{k'}(r)\times\left(\frac{-e^2}{\varepsilon\sqrt{r^2+z^2}}\right). \tag{A1}$$

Using Eq. (2.9) and the following integral representation:[52]

$$\frac{1}{\sqrt{r^2+z^2}}=\frac{2}{\pi}\int_0^{\infty}d\alpha\cos(\alpha z)K_0(\alpha r) \tag{A2}$$

gives

$$V_{kk'}=N_kN_{k'}\int_0^\infty d\alpha\left\{\int\int dz_e dz_h f_e^2(z_e)f_h^2(z_h) \times\cos[\alpha(z_e-z_h)]\int_0^R drrJ_0(kr)J_0(k'r)K_0(\alpha r)\right\}. \tag{A3}$$

The integrals over z_σ $[\sigma\in(e,h)]$ are analytic and thus pose no computational difficulty. There is, however, no closed-form solution to the integral over r, and these integrals are computationally expensive. However, there is an analytical expression in the limit of $R\to\infty$. Thus for large R,

$$\int_0^R drrJ_0(kr)J_0(k'r)K_0(\alpha r) \simeq\int_0^\infty drrJ_0(kr)J_0(k'r)K_0(\alpha r) =(k^4+\alpha^4+k'^4-2k^2k'^2+2k^2\alpha^2+2\alpha^2k'^2)^{-1/2}. \tag{A4}$$

Now let us index the in-plane wave numbers k and k', with integers i and j, respectively, with the ground state corresponding to $i=0$. We then find that for wave numbers $k=k_i$ and $k'=k_j$ where $|i-j|>30$, the approximation of Eq. (A4) is very accurate. However, for $|i-j|\leqslant 30$, the approximation does not provide accurate results and the integral in Eq. (A3) must be solved numerically. By using the above approximation, 90% of calculation burden of Coulomb matrix elements can be reduced.

APPENDIX B: MATRIX REPRESENTATION OF THE FULL HAMILTONIAN

We write the SL Hamiltonian in terms of the two-well Hamiltonian as follows:

$$H_0(z_e,z_h,r)=H_j^{TW}(z_e,z_h,r)+\Delta_j(z_e,z_h)+eF(z_e-z_h), \tag{B1}$$

where the lattice potential is given by

$$\Delta_j(z_e,z_h)=-V_e\sum_{n\neq j}R(L;z_e-nd)-V_h\sum_{n\neq 0}R(L;z_h-nd). \tag{B2}$$

Thus the matrix elements can be written as

$$(H_0)_{ij}^{\alpha\beta}=\sum_m\left[\langle\Phi_{i\alpha}^m|\Phi_{j\beta}^0\rangle E_{j\beta}^{TW}+\langle\Phi_{i\alpha}^m|\Delta_j(z_e,z_h)|\Phi_{j\beta}^0\rangle\right. \tag{B3}$$

$$\left.+eF(\langle\Phi_{i\alpha}^m|z_e|\Phi_{j\beta}^0\rangle-\langle\Phi_{i\alpha}^m|z_h|\Phi_{j\beta}^0\rangle)\right], \tag{B4}$$

where $E_{j\beta}^{TW}$ is the two-well eigenenergy. The first matrix element in Eq. (B3) is

$$\langle\Phi_{i\alpha}^m|\Phi_{j\beta}^0\rangle=\int_{-\infty}^\infty dz_e f_e[z_e-(i+m)d]f_e(z_e-jd) \times\int_{-\infty}^\infty dz_h f_h(z_h-md)f_h(z_h)D_{ij}^{\alpha\beta}, \tag{B5}$$

where

$$D_{ij}^{\alpha\beta}\equiv\sum_k A_k^{i\alpha}A_k^{j\beta}, \tag{B6}$$

and the relation

$$N_kN_{k'}\int rdrJ_0(kr)J_0(k'r)=\delta_{k,k'} \tag{B7}$$

has been used.

The other matrix elements in Eq. (B3) are given, respectively, as

$$\begin{aligned}\langle\Phi_{i\alpha}^m|\Delta_j(z_e,z_h)|\Phi_{j\beta}^0\rangle &=-D_{ij}^{\alpha\beta}\left\{V_e\sum_{n\neq j}\int_{nd-L/2}^{nd+L/2}dz_e\right.\\ &\times f_e[z_e-(i+m)d]f_e(z_e-jd)\\ &\times\int_{-\infty}^\infty dz_h f_h(z_h-md)f_h(z_h)+V_h\sum_{n\neq 0}\int_{-\infty}^\infty dz_e\\ &\times f_e[z_e-(i+m)d]f_e(z_e-jd)\\ &\left.\times\int_{nd-L/2}^{nd+L/2}dz_h f_h(z_h-md)f_h(z_h)\right\}\end{aligned} \tag{B8}$$

and

$$\begin{aligned}eF\sum_m&\left(\langle\Phi_{i\alpha}^m|z_e|\Phi_{j\beta}^0\rangle-\langle\Phi_{i\alpha}^m|z_h|\Phi_{j\beta}^0\rangle\right)\\ &=D_{ij}^{\alpha\beta}\left\{eF\int_{-\infty}^\infty dz_e f_e[z_e-(i+m)d]z_e f_e(z_e-jd)\right.\\ &\times\int_{-\infty}^\infty dz_h f_h(z_h-md)f_h(z_h)\int_{-\infty}^\infty dz_e f_e[z_e-(i+m)d]\\ &\left.\times f_e(z_e-jd)\int_{-\infty}^\infty dz_h f_h(z_h-md)z_h f_h(z_h)\right\}.\end{aligned} \tag{B9}$$

The important thing to note is that all of the matrix elements are analytic. In particular, due to our in-plane basis choice, the in-plane integrals simply reduce to the same $D_{ij}^{\alpha\beta}=\Sigma_k A_k^{i\alpha}A_k^{j\beta}$ which can be calculated once and tabulated. Thus once the two-well states have been calculated, the calculation of the BSSL eigenstates is very efficient.

APPENDIX C: CONVERGENCE IN ABSORPTION AND DYNAMICS CALCULATIONS

In studying the effect of the HIES on the intraband dynamics of the BSSL system, it is helpful to have a description of the nature of the excitonic states in a BSSL. This allows us to determine how many HIES are required to achieve convergence in both absorption and dynamics calculations. The dependence of the intraband polarization on the number of HIES and the number of wells $(2N+1)$ to be included can be understood via reference to Fig. 6. First, we introduce a convenient way of labeling the excitonic states. When the $1s$ exciton basis is used, excitonic states are described by the index $n=\ldots,-1,0,1,2,\ldots$ which is called the $1s$ excitonic WSL index. For these states, the intraband dipoles in the z direction are roughly ned, just like for the single-particle WSL states with index n. In Fig. 6, these indices n correspond to the numbers under different wells. In the full excitonic basis, each state is labeled with μ as in Eq. (2.12). In an approximate labeling scheme, the μth state can be loosely referred to as mth s-symmetry state with WSL index n. Of course, this labeling is only an approximation, since the mth s-symmetry two-well states with different j are mixed by the superlattice potential (leading, for example, to Fano resonances). The physical picture of labeling states by m and n will prove very useful in what follows. For simplicity, the laser energy E_c is assumed to be $E_c=\hbar\omega_0+2\hbar\omega_B$ for all three cases in Fig. 6.

In Fig. 6(a), only $1s$ excitons are considered. Due to the limited spectral width of the optical pulse ($\sim$25 meV), the superposition state is formed from only three WSL states $(\mu=1,2,3)$ by the exciting laser. Note that in this case the index μ reduces exactly to the $1s$ excitonic WSL index n. In Fig. 6(b), more HIES, e.g., up to 20 s, are included in the diagram. In this case, further addition of the HIES beyond 20 s in the quantum wells indexed by $n\geqslant 1$ would not have any effect on the dynamics of the system, because these newly added states are not in resonance with the laser energy. However, inclusion of still higher-energy HIES in other wells indexed by $n<1$ will influence the dynamics because some of these newly added states will fall within the spectral width of the exciting laser. In other words, the configuration in Fig. 6(b) still does not lead to a converged result. Finally, in Fig. 6(c), the HIES included are more than enough for a converged result. In practice, to obtain a converged result for the system and fields investigated in this work, the highest in-plane state should be around 60 s. Note that although HIES greater than 60 s for, say, $n=-10$ will be in resonance, they have a negligible absorption strength due to the large electron-hole separation, and hence need not be included in the basis. Another factor that influences the convergence is the number of wells included in the calculation. It is found that $2N+1=13$ wells are enough for the calculations of intraband polarization or the terahertz emission for moderate electric-field strength ($\sim$15 kV/cm). Further inclusion of new wells will not change the results because the M_μ for states with large j are negligible due to the small overlap between the electron and hole for these two-well states. For

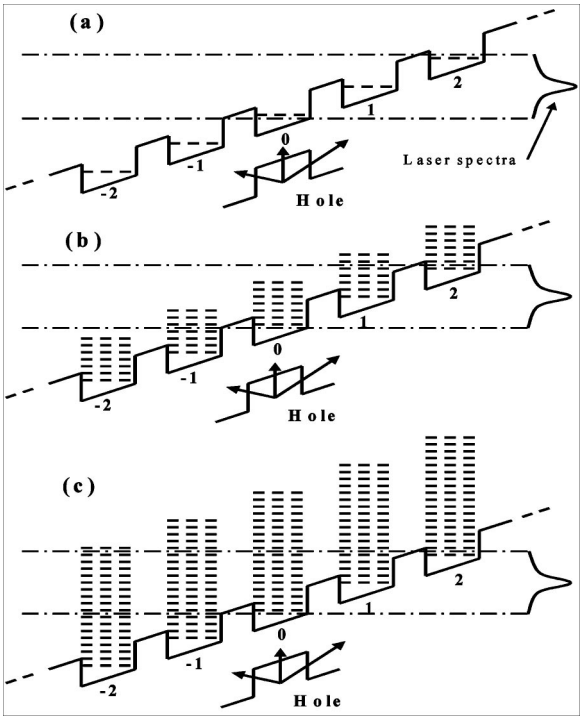

FIG. 6. Schematic diagrams for the inclusion of different number of higher in-plane excitonic states in the dynamics simulation. For simplicity, the hole is considered localized in the $n=0$ well. The exciting short-pulse laser spectrum is shown on the right. The three figures show schematically the effect of adding HIES to the two-well basis.

$F=0$, however, because the exciton states are no longer localized as in the finite F case, we need a total number of $2N+1=31$ wells for convergence.

APPENDIX D: INTERBAND AND INTRABAND DIPOLE MATRIX ELEMENTS

By substituting the exciton envelope function of Eq. (2.12) into Eq. (3.8), the interband dipole matrix elements are written as

$$\mathbf{M}_\mu=\mathbf{M}_0\sqrt{A(2N+1)}\int dz\,\psi^{\mu}{}^*(z_e=z,z_h=z,r=0)$$
$$=\mathbf{M}_0\sum_{j=-N}^{N}\sum_{\alpha=1}^{M}\sum_k C_{j\alpha}^{\mu}N_kA_k^{j\alpha}\int dz f_e(z)f_h(z-jd). \tag{D1}$$

The calculation of intraband dipole matrix elements is much more complicated than in the $1s$ exciton case. The explicit form intraband dipole matrix element is

$$\mathbf{G}_{\mu\mu'}=\langle\psi^{\mu}|-e(z_e-z_h)|\psi^{\mu'}\rangle$$
$$=-\frac{e}{2N+1}\sum_{ij\alpha\alpha'}C_{i\alpha}^{\mu}C_{j\beta}^{\mu'}S_{ij}D_{ij}^{\alpha\beta}, \tag{D2}$$

where

$$S_{ij} \equiv \sum_{mm'} \left\{ \int dz_h f_h[z_h-(i+m)d] f_h[z_h-(j+m')d] \int dz_e f_e(z_e-md) z_e f_e(z_e-m'd) - \int dz_e f_e(z_e-md) f_e(z_e-m'd) \right.$$
$$\left. \times \int dz_h f_h[z_h-(i+m)d] z_h f_h[z_h-(j+m')d] \right\} \tag{D3}$$

can be calculated analytically, and the $D_{ij}^{\alpha\beta}$ are defined in Eq. (B6) in Appendix B.

[1] F. Bloch, Z. Phys. **52**, 555 (1928).
[2] Hubert M. James, Phys. Rev. **76**, 1611 (1949).
[3] G. H. Wannier, *Elements of Solid State Theory* (Cambridge University Press, London, 1959), p. 190.
[4] G.H. Wannier, Phys. Rev. **117**, 432 (1969).
[5] See, for example, J. M. Ziman, *Principles of the Theory of Solids*, 2nd ed. (Cambridge University Press, London, 1972), p. 191.
[6] L. Esaki and R. Tsu, IBM J. Res. Dev. **14**, 61 (1970).
[7] E.E. Mendez, F. Agulló-Rueda, and J.M. Hong, Phys. Rev. Lett. **60**, 2426 (1988).
[8] J. Feldmann, K. Leo, J. Shah, D.A.B. Miller, J.E. Cunningham, T. Meier, G. von Plessen, A. Schulze, P. Thomas, and S. Schmitt-Rink, Phys. Rev. B **46**, 7252 (1992).
[9] K. Leo, P. Haring Bolivar, F. Brüggemann, R. Schwedler, and K. Köhler, Solid State Commun. **84**, 943 (1992).
[10] C. Waschke, H.G. Roskos, R. Schwedler, K. Leo, H. Kurz, and K. Köhler, Phys. Rev. Lett. **70**, 3319 (1993).
[11] V.G. Lyssenko, G. Valušis, F. Löser, T. Hasche, K. Leo, M.M. Dignam, and K. Köhler, Phys. Rev. Lett. **79**, 301 (1997).
[12] S. Schmitt-Rink and D.S. Chemla, Phys. Rev. Lett. **57**, 2752 (1986).
[13] S. Schmitt-Rink, D.S. Chemla, and H. Haug, Phys. Rev. B **37**, 941 (1988).
[14] M. Lindberg and S.W. Koch, Phys. Rev. B **38**, 3342 (1988).
[15] M. Lindberg, R. Binder, and S.W. Koch, Phys. Rev. A **45**, 1865 (1992).
[16] T. Meier, F. Rossi, P. Thomas, and S.W. Koch, Phys. Rev. Lett. **75**, 2558 (1995).
[17] V.M. Axt and A. Stahl, Z. Phys. B: Condens. Matter **93**, 195 (1994); K. Victor, V.M. Axt, and A. Stahl, Phys. Rev. B **51**, 14 164 (1995).
[18] V.M. Axt, G. Bartels, and A. Stahl, Phys. Rev. Lett. **76**, 2543 (1996).
[19] Th. Östreich, K. Schönhammer, and L.J. Sham, Phys. Rev. B **58**, 12 920 (1998).
[20] Th. Östreich, N. Donlagic, C. Wohler, and K. Schönhammer, Phys. Status Solidi B **206**, 205 (1998).
[21] Jörg Hader, Torsten Meier, Stephan W. Koch, Fausto Rossi, and Norbert Linder, Phys. Rev. B **55**, 13 799 (1997).
[22] R. Binder, S.W. Koch, M. Lindberg, W. Schäfer, and F. Jahnke, Phys. Rev. B **43**, 6520 (1991).
[23] G. Bartels, G.C. Cho, T. Dekorsy, H. Kurz, A. Stahl, and K. Köhler, Phys. Rev. B **55**, 16 404 (1997).
[24] C. Sieh, T. Meier, F. Jahnke, A. Knorr, S.W. Koch, P. Brick, M. Hübner, C. Ell, J. Prineas, G. Khitrova, and H.M. Gibbs, Phys. Rev. Lett. **82**, 3112 (1999); C. Sieh, T. Meier, A. Knorr, F. Jahnke, P. Thomas, and S.W. Koch, Eur. Phys. J. B **11**, 407 (1999).
[25] T. Meier, S.W. Koch, P. Brick, C. Ell, G. Khitrova, and H.M. Gibbs, Phys. Rev. B **62**, 4218 (2000).
[26] Thomas Östreich, Phys. Rev. B **64**, 245203 (2001).
[27] J.M. Lachaine, Margaret Hawton, J.E. Sipe, and M.M. Dignam, Phys. Rev. B **62**, R4829–R4832 (2000).
[28] W. Schäfer, D.S. Kim, J. Shah, T.C. Damen, J.E. Cunningham, K.W. Goossen, L.N. Pfeiffer, and K. Köhler, Phys. Rev. B **53**, 16 429 (1998).
[29] Wei Min Zhang, Torsten Meier, Vladimir Chernyak, and Shaul Mukamel, Phys. Rev. B **60**, 2599 (1999).
[30] M.M. Dignam and M. Hawton, Phys. Rev. B **67**, 035329 (2003).
[31] M. Hawton and M.M. Dignam, Phys. Rev. Lett. **91**, 267402 (2003).
[32] U. Fano, Phys. Rev. **124**, 1866 (1961).
[33] M.M. Dignam and J.E. Sipe, Phys. Rev. Lett. **64**, 1797 (1990); Phys. Rev. B **43**, 4097 (1991).
[34] D.M. Whittaker, Europhys. Lett. **31**, 55 (1995).
[35] S. Glutsch and F. Bechstedt, Phys. Rev. B **57**, 11 887 (1998).
[36] H. Chu and Y.-C. Chang, Phys. Rev. B **36**, 2946 (1987).
[37] G. Mo and C.C. Sung, Phys. Rev. B **38**, 1978 (1988).
[38] W.T. Masselink, P.J. Pearah, J. Klem, C.K. Peng, H. Morkoç, G.D. Sanders, and Y.C. Chang, Phys. Rev. B **32**, 8027 (1985).
[39] N. Linder, Phys. Rev. B **55**, 13 664 (1997).
[40] Hartmut G. Roskos, Christian Waschke, Ralf Schwedler, Patrick Leisching, Youssef Dhaibi, Heinrich Kurz, and Klaus Köhler, Superlattices Microstruct. **15**, 281 (1994).
[41] Y. Shimada, K. Hirakawa, and S.-W. Lee, Appl. Phys. Lett. **81**, 1642 (2002).
[42] M.M. Dignam and J.E. Sipe, Phys. Rev. B **41**, 2865 (1990).
[43] Jean-Marc Lachaine, MSc. thesis, Lakehead University, 2002.
[44] C.P. Holfeld, F. Löser, M. Sudzius, K. Leo, D.M. Whittaker, and K. Köhler, Phys. Rev. Lett. **81**, 874 (1998).
[45] M. Dignam, J.E. Sipe, and J. Shah, Phys. Rev. B **49**, 10 502 (1994).
[46] F. Löser, M.M. Dignam, Yu.A. Kosevich, K. Köhler, and K. Leo, Phys. Rev. Lett. **85**, 4763 (2000).
[47] Q. Wu and X.-C. Zhang, Appl. Phys. Lett. **68**, 1604 (1996).
[48] Q. Wu and X.-C. Zhang, Appl. Phys. Lett. **71**, 1285 (1997).
[49] A. Leitenstorfer, S. Hunsche, J. Shah, M.C. Nuss, and W. H Knox, Appl. Phys. Lett. **74**, 1516 (1999).
[50] Paul C.M. Planken, Igal Brener, Martin C. Nuss, M.S.C. Luo, S.L. Chuang, and L.N. Pfeiffer, Phys. Rev. B **49**, 4668 (1994).
[51] R. Martini, G. Klose, H.G. Roskos, H. Kurz, H.T. Grahn, and R. Hey, Phys. Rev. B **54**, R14 325 (1996).
[52] See, for example, John David Jackson, *Classical Electrodynamics*, 3rd ed. (Wiley, New York, 1999).